Article

A TiO2/g-C3N4/CdS Nanocomposite-Based Photoelectrochemical Biosensor for Ultrasensitive Evaluation of T4 Polynucleotide Kinase Activity

Pan-Pan Li, Yue Cao, Chang-Jie Mao, Baokang Jin, and Jun-Jie Zhu

Anal. Chem., **Just Accepted Manuscript** • DOI: 10.1021/acs.analchem.8b04823 • Publication Date (Web): 18 Dec 2018

A TiO_2/g-C_3N_4/CdS Nanocomposite-Based Photoelectrochemical Biosensor for Ultrasensitive Evaluation of T4 Polynucleotide Kinase Activity

Pan-Pan Li [a,b], Yue Cao [b], Chang-Jie Mao [a,*], Bao-Kang Jin [a], Jun-Jie Zhu [b,*]

[a] *Anhui Province Key Laboratory of Chemistry for Inorganic/Organic Hybrid Functionalized Materials, School of Chemistry and Chemical Engineering, Anhui University, Hefei 230601, PR China*

[b] *State Key Laboratory of Analytical Chemistry for Life Science, School of Chemistry and Chemical Engineering, Nanjing University, Nanjing 210023, PR China*

Pan-Pan Li and Yue Cao contributed equally to this work

ABSTRACT

Herein, an efficient photoelectrochemical (PEC) platform was constructed by a co-sensitization strategy with a cascade energy level arrangement for the ultrasensitive evaluation of T4 polynucleotide kinase (T4 PNK). Based on CdSe quantum dots (QDs) with an extremely narrow bandgap, this co-sensitization strategy offered a highly efficient sensitizer with a matching band-edge level of a ternary TiO_2/g-C_3N_4/CdS nanocomposite. In this protocol, the ternary nanocomposite was first prepared to serve as the matrix to construct the PEC sensing platform. On the other hand, a well-designed hairpin DNA_1 probe with 5'-hydroxyl termini was specifically phosphorylated by T4 PNK which would be selectively cleaved with lambda exonuclease (λ-Exo) outputting 3'-thiol end $ssDNA_2$. After tagged with CdSe QDs, $ssDNA_2$ was captured by the complementary capture DNA_3 on the electrode surface. As a result, CdSe QDs were in close contact with the ternary nanocomposite matrix, leading to an enhanced photocurrent response. Therefore, this proposed PEC platform displayed an analytical performance with a wide linear range from 0.0001 to 0.02 U mL^{-1} and a low detection

limit down to 6.9×10^{-5} U mL^{-1}. Moreover, this ternary nanocomposite-based platform exhibited excellent selectivity, good reproducibility, and remarkable storage stability, which shows the great potential for the T4 PNK detection and inhibitor screening.

INTRODUCTION

T4 PNK, as a primary member of the 5'-kinase family which can catalyze the transfer of γ-phosphate group of nucleoside triphosphate to the 5'-hydroxyl termini of nucleic acids or oligonucleotides,[1,2] was first discovered in 1965.[3] The aberrant activity of T4 PNK results in many lethal illnesses, such as loom's, Rothmund-Thomson and Werner's syndromes.[4,5] Therefore, monitoring T4 PNK activity is very meaningful and significant for kinase-targeted drug discoveries, clinical diagnoses, as well as fundamental biochemical processes.[6-8] The conventional T4 PNK measurements mainly utilize the analytical techniques including autoradiography, electrophoresis, and ^{32}P labeling, but suffer from several weaknesses including complicated operating procedures, time consuming, and perilous radioactivity.[9-11] To overcome these drawbacks, many strategies including electrochemistry,[12] colorimetry,[13] fluorescence,[11,14] and other methods[15] have been proposed to monitor T4 PNK activity and inhibition. Fluorescence strategies have emerged as the most popular method to detect T4 PNK activity. For example, Hou's group[14] proposed a catalyzed hairpin assembly-mediated target recycling amplification strategy for the ultrasensitive measurement of T4 PNK activity. Lin's[16] group took advantage of the hyper quenching property of graphene oxide to evaluate the T4 PNK activity. Great efforts have already been devoted, however, the sensitivity evaluation for T4 PNK activity still remains a

big challenge.[11,16]

Recently, PEC detection technology with multiple advantages, including sensitivity, cheap instrumentation with simple operation and a wide dynamic range,[17] has been widely applied to immunoassay[18,19], genosensor[20] and cytosensor.[21] The PEC reaction describes a photoelectric conversion process involving the charge separation and transfer of photoactive materials under the illumination of a light source.[17,20] Semiconductor nanomaterials are recognized as the most widely utilized photoactive materials due to their special electronic states of valence band (VB) and conduction band (CB), as well as the suitable band gap. Taking the n-type semiconductor as an example, the electrons on the VB of the semiconductor photoactive species are excited by the light and then skip the band gap from VB to CB, resulting in the separated electrons in CB and the remained holes in VB.[17,22] The photoexcited electrons transfer to the electrode and support an stable electrical signal readout. The PEC biosensing is conducted by recording the changed photocurrent responses caused by the interaction between the photoactive species and target, and this alteration shows a close relationship with the analyte dose.[17-22] Therefore, A PEC biosensor shows inherent superiority with negligible background due to its total separated energy forms of the visible light as a non-intrusive excitation source and the photoelectric outputs as detection signals.[22] It is worth noting that, to date, no PEC platform has been constructed for sensitively detecting the activity of T4 PNK-catalyzed phosphorylation reaction.

Generally, the performance of PEC biosensors depends heavily on the features of the

photoactive materials. Among a variety of photoactive materials, TiO_2 has been confirmed as a basic material to develop PEC bioassays because of its strong photocatalytic activity, good biocompatibility, chemical stability and controllable morphology.[23] Unfortunately, TiO_2 can only be excited by ultraviolet light (<387 nm), thereby wasting more than 95% of the solar light spectrum.[24] Even worse, the fast recombination of photo-induced electron and hole usually leads to a relatively low PEC signal, which greatly restricts its practical use.[25]

To address these issues, the binary nanocomposites by hybridizing TiO_2 with narrow bandgap semiconductors such as graphitic C_3N_4 (g-C_3N_4, ~2.7 eV)[26-28], CdS (~2.4 eV)[29], MoS_2 (~1.9 eV)[30], CdSe (~1.8 eV)[31] and CdTe (~1.56 eV)[32] have been exploited to improve the photoelectric response extending to visible region. These narrow band gap semiconductors serve as sensitizers because their conduction bands (CBs) is higher than those of TiO_2, promoting the flow of photogenerated electrons from their CB to the CB of TiO_2, which assists in charge separation and enhances the PEC ability of the TiO_2-based nanocomposite.[33] To further improve the performance of PEC, these co-sensitized structures are more sophisticatedly designed, leading to the development of nanocomposites with two or more different energy gap sensitizers such as $TiO_2/Ag_2S/Bi_2S_3$[34], TiO_2/MoS_2/AuNPs.[35] Herein, a ternary TiO_2/g-C_3N_4/CdS nanocomposite was first prepared by coupling TiO_2 with two narrow bandgap semiconductors to form co-sensitized structures with stepwise band-edge levels, which not only increased the light absorption capacity, but also effectively prevented charge recombination, accordingly improving photoelectric conversion efficiency. Therefore,

this novel ternary nanocomposite could qualify for PEC electrode matrix to obtain a strong and stable photocurrent signal under white light illumination.

Strategies based on co-sensitization signal amplification are constantly implemented to construct PEC biosensor.[36] These strategies are based on a co-sensitization effect arising from narrow band gap semiconductors as sensitizers in close contact with the electrode matrix material to form co-sensitized structures. These sensitizers can expand the absorption region of the matrix enduing the system with a superior light absorption capacity. Besides, the sensitizers exhibit higher CBs than the matrix materials do, promoting the flow of photo-generated electrons from their CBs to the CBs of the matrix materials, which accelerate charge separation and transfer. Therefore, the effects of the co-sensitization strategy including sufficient light absorption, effective charge separation, and rapid electron transfer can improve the PEC ability to supply an enhanced photocurrent readout. The co-sensitization strategy is simple and cost-effective enough to construct a PEC platform compared to a more conventional method involving the use of enzymes, which usually bears a hindered charge transfer, and a high cost and time consuming procedure.[37] Apparently, the efficiency of co-sensitization effect determines analytical performance but it is affected by the electrode matrix material and sensitizers. CdSe QDs as an extremely narrow bandgap semiconductor could match well with the ternary nanocomposite with cascade energy level arrangement to achieve high co-sensitization efficiency. To the best of our knowledge, however, a ternary nanocomposite has not yet been constructed and utilized to co-sensitize with CdSe QDs within a PEC platform.

Therefore, in our work, we take advantages of the highly efficient co-sensitization strategy to sensitively detect T4 PNK activity. As depicted in Scheme 1A, the efficiency of phosphorylation process through catalyzing a 5'-hydroxyl group terminal hairpin DNA_1 to form a phosphate group was utilized to assess the T4 PNK activity. Then, lambda exonuclease (λ-Exo) selectively catalyzed the progressive hydrolysis of double-stranded DNA (dsDNA) sequence from 5'-PO_4 terminal to release single nucleotides to output a 3'-thiol ssDNA_2. Finally, DNA_2 labelled with CdSe QDs (DNA_2-CdSe QDs) was hybridized with the exposed DNA_3 on the electrode surface forming a co-sensitization structure to trigger an enhanced photocurrent for accurate measurement of T4 PNK activity. Such a construct provides a novel approach for designing reliable and sensitive PEC sensors for the T4 PNK activity evaluation and inhibitor screening.

EXPERIMENTAL SECTION

Materials and Instruments

All the materials and instruments utilized in this work were supplied in Supporting Information.

Preparation of Ternary Nanocomposites

The ternary TiO_2/g-C_3N_4/CdS nanocomposite was synthesized in two steps. The first step was to synthesize a binary TiO_2/g-C_3N_4 complex using a modified method.[38] Typically, a mixture of 10 g urea and 2 g TiO_2 in 20 mL deionized water was stirred for 1 h. After that, the precipitation was dried thoroughly at 80 ºC. The solid powder was packed in 4 sheets of aluminum foil, and calcined in a muffle at 550 ºC for 3 h with a rate of 5 ºC/min. The polymerization space of g-C_3N_4 was highly limited with the assistance of the 4 layers aluminum foil so that the g-C_3N_4 shell could be synthesized covering TiO_2 in situ in the heating procedure.[38] The second part was to decorate CdS QDs on the surface of binary complex in situ. Specifically, 40 mg of binary nanocomposite was uniformly dispersed in 40 mL pure water followed by adding 0.15 g of $CdCl_2$. The dispersion was bubbled with nitrogen (N_2) for a quarter, and its pH was adjusted to eleven through dropwise addition of NaOH solution (1 M) followed which 40 mL of 20 mM TAA were successively added in. Afterwards, this prepared reaction solution was refluxed for 2 h (80 ºC) under N_2 protection. After being treated with anhydrous ethanol, the compounds were centrifuged at 8500 rpm for ten minutes and rinsed with distilled water three times. Eventually, this acquired water-soluble ternary

TiO_2/g-C_3N_4/CdS nanocomposite was redistributed in distilled water and stored at 4 ºC.

Fabrication of a T4 PNK Sensing Platform

The fluorine-doped tin oxide (FTO) glass was cut into small stripe pieces (5 mm × 9 mm) and was sequentially sonicated in distilled water, acetone and ethanol. The manufacture process was schematically exhibited in Scheme 1A. Firstly, Poly dimethyl diallyl ammonium chloride (PDDA) was utilized to treat the surface of FTO glass with positive charge by applying PDDA (30 μL, 2%) on the surface for one hour. After being washed with distilled water and dried in a N_2 atmosphere, a 30 μL aqueous dispersion of TiO_2/g-C_3N_4/CdS nanocomposite was utilized to modify the FTO surface. After the material was completely solidified on the surface of FTO, the T4 PNK sensing platform was finally constructed by bio-functionalizing the ternary nanocomposite with capture DNA_3. Specifically, the capture DNA_3 solution was pretreated by tris-(2-carboxyethyl)-phosphine (TCEP, 100 mM) to open the S-S bonds. Afterwards, 30 μL capture DNA_3 solution (1 μM) was applied on the ternary nanocomposite matrix at 4 ºC overnight. After the electrode was rinsed with TE buffer (10 mM Tris-HCl solution containing 1 mM EDTA) and dried under N_2 atmosphere, 30 μL 6-mercaptohexanol (MCH, 10 mM) was used to detach the unbinding capture DNA_3 and block the remaining active sites.

Evaluation of T4 PNK Activity

The PEC detection was conducted at room temperature in 10 mM phosphate buffer solution (PBS) containing 0.1 M ascorbic acid (AA), which provides sufficient electrons to improve PEC performance. A Xenon Lamp with full spectrum irradiation was used as the excitation light source. The PEC detection process was also

schematically exhibited in Scheme 1A. Firstly, a hairpin DNA_1 solution (1 μM) was annealed to form a hairpin structure prior to use. Typically, hairpin DNA_1 (1 μM) was dispersed in TE buffer with 1.5 mM $MgCl_2$ at a volume ratio of 100:1. The hairpin DNA_1 solution was then annealed by heating to 90 ºC and cooling down to room temperature. Then it was pretreated by TCEP (100 mM) for 1 h to break disulfide bonds. Crucially, the phosphorylation system was applied to evaluate T4 PNK activity by the quantitatively evolution of the conversion from 5'-hydroxyl group to 5'-phosphate group of hairpin DNA_1, which contains 5 μL of hairpin DNA_1 (1 μM), 3.6 μL of reaction buffer A (500 mM Tris-HCl solution containing 10 mM $MgCl_2$, 50 mM DTT, and 1 mM EDTA), 0.5 μL of ATP (100 mM) and various concentrations of T4 PNK for a one-hour incubation. After that, 0.35 μL of λ-Exo (10 U μL^{-1}) diluted with PBS was mixed with the solution while being incubated at 37 ºC for 50 minutes to sequentially cleave DNA_1 from 5'-PO_4 terminal. In our work CdSe QDs was synthesized and activated as previous reported[37] (*Synthesis of CdSe QDs* and Figure S1, Supporting Information). After incubating with 10 μL CdSe QDs at 37 ºC for 1 hour, the solution was finally applied on the sensing platform with capture DNA_3 to facilitate the DNA hybridization reaction to achieve co-sensitized structure. Finally, the FTO electrode served as a working electrode to collect corresponding photocurrent signal.

Screening T4 PNK inhibitor

$(NH_4)_2SO_4$ and adenosine diphosphate (ADP) are typical models for inhibition of T4 PNK catalyzed phosphorylation process.[11,14,39] Different amounts of inhibitors were employed in the phosphorylation system with an ultimate T4 PNK concentration at 1.0

U mL^{-1}. With the exception of increasing the incubation time to one hour, the other parameters were identical to those specified above.

RESULTS AND DISCUSSION

Characterization of Ternary Nanocomposite

Scanning electron microscopy (SEM) and transmission electron microscopy (TEM) were utilized to characterize the morphology of the ternary TiO_2/g-C_3N_4/CdS nanocomposite. Figure 1A displays the scanning electron micrograph exhibiting a three-dimensional structure with fluffy stereoscopic morphology, which is favorable to the absorption of light. Figure 1B1 exhibits the transmission electron micrograph with tightly packed titanium dioxide structure covered by g-C_3N_4 sheets, suggesting that TiO_2 compacts well with g-C_3N_4 and changes its morphology. As shown in Figure 1B2 and 1B3, the transmission electron micrographs show the standard morphology of nanocomposite, and high-revolution transmission electron micrograph exhibits lattice fringes corresponding to the interplanar distance of 0.31 and 0.25 nm which can be ascribed to the (101) plane of TiO_2 and (111) plane of CdS QDs, respectively.[38,40]

X-ray powder diffraction (XRD), elemental mapping and X-ray photoelectron spectroscopy (XPS) were also conducted to demonstrate the successful synthesis of the ternary nanocomposite. Figure 1C presents the XRD data of TiO_2 alone. TiO_2/g-C_3N_4, and TiO_2/g-C_3N_4/CdS nanocomposite. The diffraction peaks (2θ values) of TiO_2/g-C_3N_4 at 25.28°, 37.80°, 48.05°, 55.06°, 62.69°, 70.31°, 76.01°, and 82.66° matched well with the (101), (004), (200), (211), (204), (220), (301), and (224) planes of pure TiO_2 (JCPDS card no. 21-1272), indicating that the crystalline characteristics of TiO_2 nanoparticles remained unchanged after reaction. Sharp peaks in the pattern of TiO_2/g-

C_3N_4/CdS with 2θ values at 26.52°, 43.96°, and 52.13° could be ascribed to the (111), (220), and (311) planes of CdS, which was consistent with the previous work reported by Maity et al.,[40] indicating good crystalline characteristics of CdS QDs on the surface of TiO_2/g-C_3N_4. The result implied that CdS, g-C_3N_4 and TiO_2 crystal structures were indeed in existence in this ternary nanocomposite. The elemental mapping images displayed the existence of Ti, N, and Cd elements within the ternary nanocomposite, indicating the successful synthesis (Figure 1D). In addition, Figure S2 (Supporting Information) shows the survey XPS spectrum of the three materials. Elements including O, Ti, Cd, N, C, and S were displayed in this ternary nanocomposite, further revealing the coexistence of these three components.

Feasibility of Co-sensitization Amplification Strategy

To explore the feasibility and mechanism of the co-sensitization amplification strategy, three kinds of materials including pristine TiO_2, binary TiO_2/g-C_3N_4 complex and the ternary TiO_2/g-C_3N_4/CdS nanocomposite were used as matrixes for constructing the electrodes. The photocurrent response from the three systems were examined by casting constant amounts of CdSe to form co-sensitized structure (Figure 2). The corresponding co-sensitization efficiency (E) was calculated on the basis of $E = (I_i/I_0 - 1) \times 100\%$, where I_0 and I_i respectively represents the photocurrent before and after co-sensitization with CdSe QDs sensitizers. The corresponding co-sensitization amplification efficiency of the three matrixes was 50%, 65% and 89%. Experimental data demonstrated the co-sensitization effect between ternary nanocomposite and CdSe QDs exhibiting the highest efficiency. This phenomenon was mainly based on the matching of the extremely narrow bandgap of CdSe QDs with the stepwise band-edge levels of the ternary nanocomposite, making it a competent as sensitizer to achieve a high co-sensitization efficiency. Thus, the proposed PEC biosensor based on co-sensitization

amplification strategy by coupling CdSe QDs with ternary TiO_2/g-C_3N_4/CdS nanocomposite is feasible with achievable high sensitivity. This issue was also verified with XPS technology.

XPS spectra were acknowledged as convincing supplementary evidence to identify the valence elements and explain the electron transport by studying the shift in the binding energy of elements. As shown in Figure 3a, two remarkable peaks of Ti were clearly observed at 459.30 eV (Ti $2p_{1/2}$), 465.05 eV (Ti $2p_{3/2}$), and the splitting between them of our three TiO_2-based materials were 5.75 eV, suggesting the normal state of Ti^{4+}. This inference was according to the article reported by Tang et al. that the splitting binding energy between Ti $2p_{1/2}$ and Ti $2p_{3/2}$ is 5.7 eV suggesting the normal state of Ti^{4+}.[41] However, the typical binding energy of Ti has obviously shifted to a lower state after forming a ternary nanocomposite. The oxygen peak (Figure 3b) located at 530.55 eV corresponds to Ti-O groups, and a similar positive shift of binding energy was observed after the formation of compounds. As shown in Figure 3c, the typical binding energy of g-C_3N_4 at 284.80 and 288.70 eV in the C 1s spectrum correspond to that of C-$(N)_3$, and N-C=N, respectively. Moreover, both C 1s and N 1s peaks moved to a lower binding energy in the ternary nanocomposite (Figure 3c, d). As exhibited in Figure 3e, Cd 3d region shows two typical peaks at 404.95 eV ($3d_{5/2}$) and 411.65 eV ($3d_{3/2}$), and Figure 3f displays S 2p region, which could be simulated into two peaks at 161.05 eV ($2p_{3/2}$) and 162.25 eV ($2p_{1/2}$). Unlike the previous ones, both Cd 3d and S 2p migrated to a higher state. It has been confirmed that the internal electronic structure has a strong effect on the local binding energies of TiO_2, g-C_3N_4 and CdS formed a heterojunction according to those previously reported that the formed heterojunction will affect the local binding energies of the components of the compound.[31,42,43] Hence, the XPS results suggested that the components of the ternary nanocomposite are well

connected with each other by strong interactions. In addition, compared with the pure materials, local binding energies of Cd and S in ternary nanocomposite obviously shifted to higher states, but C, N, Ti and O migrated to opposite energy states. The possible reason is that there is a positive charge area on the CdS surface due to the transfer or consumption of electrons from CdS resulting in increased local binding energies of Cd and S elements, but g-C_3N_4 and TiO_2 possess negative charge domains owning to the acceptance of electrons leading to reduced local biding energies of C, N, Ti, and O elements in XPS testing. Therefore, there is an effective charge transfer inter the ternary nanocomposite and the electrons transfer path is from CdS QDs to the g-C_3N_4 surface and eventually reaching the inner layer of TiO_2 (Scheme 1B). Such electron transfer can attribute to Fermi level rearrangement when the nanocomposite meet the Fermi-Dirac distribution resulting in stepwise band edges.[44] Therefore, the ternary TiO_2/g-C_3N_4/CdS nanocomposite could be used as a matrix of PEC platform with cascade energy level arrangement to achieve highest co-sensitization efficiency, resulting in a better analytical performance to sensitively detect T4 PNK activity.

Characterization Construction and Feasibility of the PEC Platform

To evaluate the successful construction and the detection feasibility of the as-fabricated PEC platform, we made a comparison of the photocurrent at different stages of the fabrication process, and the experimental conditions were identical to those specified at *Evaluation of T4 PNK Activity* in Experimental Section. The experimental results was shown in Figure 4A. Trace a shows a low background photocurrent at a bare FTO electrode. Trace b represents the photoelectric response of the pristine TiO_2-modified the FTO electrode, and it shows a relatively low photocurrent of 15.3 μA. The weak photoelectric response is owing to the poor light absorption capacity of TiO_2 resulting

from its relatively large band gap. Meanwhile, the rapidly decreased photocurrent of trace b in the detection process from 10 to 30 seconds also indicated the fast recombination of photo-induced electron and hole between CB and VB band of TiO_2. Next, at the TiO_2/g-C_3N_4-modified the FTO electrode (trace c), the photocurrent increase to 30.7 μA because g-C_3N_4 with a narrow band gap could prevent recombination of photo-induced electron and increase the efficiency of electron transmission. Meanwhile, the photocurrent at the ternary TiO_2/g-C_3N_4/CdS nanocomposite-modified electrode (trace d) was enhanced to 95.0 μA, indicating that the photoactive material of CdS could improve the light absorption capacity and promote charge separation. However, the photocurrent decreased to 80.0 μA after attaching capture DNA_3 to the electrode and then blocking with MCH (trace e). When DNA_2-CdSe QDs hybridized onto the surface, the signal enhanced significantly to 180.0 μA (trace f), because CdSe QDs with a narrow band gap could increase the efficiency of light absorption and the impactful co-sensitization effect aided in achieving the coupling with ternary nanocomposite. As a control, the only CdSe QDs were applied on the electrode matrix without the bio-functionalization of DNA_2, and the photocurrent in trace g was measured to be 78.0 μA. The photocurrent was almost unchanged compared to trace e and largely lower compared to trace f, which seemed to indicate very little non-specific adsorption between CdSe QDs alone and the TiO_2/g-C_3N_4/CdS/MCH-modified electrode. Based on the above results, we concluded that the PEC sensing platform was successfully constructed and could be applied for ultrasensitive detection of T4 PNK activity.

Electrochemical impedance spectroscopy (EIS) has been commonly used to investigate the interfacial properties of fabricated electrode. The detailed experimental parameters were detailed at *Instruments* in Supporting Information. Typically, a semicircular shape is obtained in the high frequency range of a Nyquist plot, the diameter of which is related to the electron transfer resistance (R_{et}) of an electron reaction.[45] Figure 4B shows the impedance spectrum at different steps of the fabrication process of the PEC platform. The bare FTO electrode exhibited a small R_{et} value of 90 ohm (trace a) and the R_{et} value increased to 158 ohm (trace b) after the modification of the ternary nanocomposite, indicating its successful immobilization on the surface of electrode. After the electrode was bio-functionalized with capture DNA_3 and blocked with MCH, the R_{et} value increased to 198 ohm (trace c) because both capture DNA_3 and MCH showed low conductivity, and capture DNA_3 could form a negatively charged layer on the surface with a repelling effect toward the negatively charged ferricyanide molecules. After CdSe QDs-DNA_2 immobilized on the electrode (trace d), R_{et} value increased again to 249 ohm, which was ascribed to lower electron-transfer abilities of the CdSe QDs. It was noteworthy that sole CdSe QDs modified on the electrode displayed an unobviously changed R_{et} value of 212 ohm (trace e) compared to trace c, indicating that the nonspecific adsorption can be neglected. Therefore, these expectable change of R_{et} values suggested the successful fabrication of the T4 PNK sensing platform and this method for T4 PNK detection was completely feasible.

Optimization of Assay Conditions

Several crucial parameters including volume of ATP and λ-Exo, reaction time of T4

PNK-catalyzed phosphorylation and the integrated λ-Exo cleavage process, as well as incubation time of DNA hybridization reaction were investigated and optimized to obtain the best analytical performance of the proposed platform (Figure S3, Supporting Information). As shown in Figure S3A, the photocurrent exhibited a gradual enhancement along with the increasing volume of ATP (100 mM), and reached its maximum at the volume of 0.5 μL. Then, the photocurrent decreased because the active sites of T4 PNK for DNA might be inhibited by the excess of ATP.[16] Therefore, we chose 0.5 μL as the optimal ATP volume. The photoelectrical responses to different volume of λ-Exo (10 U μL^{-1}) showed the same trend, as shown in Figure S3B. The photocurrent reached the highest value at 0.35 μL of λ-Exo suggesting the full cleavage process. Then the photocurrent decreased obviously because the superfluous λ-Exo may cause the side reaction and affect the formation of DNA_2. Thus, 0.35 μL was chosen as the optimal volume of λ-Exo. As displayed in Figure S3C, the photocurrent increased obviously from 30 to 60 min, and then reached a platform, suggesting the complete phosphorylation. Accordingly, the perfect phosphorylation reaction time was determined to be 1 h to get the highest efficiency in the shortest time. Also, the photocurrents exhibited the same trend in the cleavage and DNA hybridization reaction process. Thus, the coupled cleavage process got a proper time at 50 min (Figure S3D), and the incubation time of DNA hybridization reaction was optimized at 60 min (Figure S3E).

Dose-Response Curves for T4 PNK

Under the optimal conditions, T4 PNK activity was evaluated by this proposed platform.

Figure 5A displays the photocurrent responses corresponding to various doses of T4 PNK. The photocurrent exhibits a gradual enhancement along with the increasing amounts of T4 PNK. Figure 5B shows the relationship between photocurrents and T4 PNK doses. The photocurrent response (I) linearly increases with increasing logarithm of T4 PNK dose ([*C*]), and the regression equation is I (μA) = $168.57 + 20.34 \lg [C]$ (U mL^{-1}) (R^2=0.9937, N = 7) with a linear concentration range between 0.0001-0.02 U mL^{-1}, and a low detection limit (based on a signal-to-noise of 3) of 6.9×10^{-5} U mL^{-1}, demonstrating that our platform exhibited excellent analytical performance to sensitively detect T4 PNK.

The analytical performance of the proposed PEC biosensor is superior to most of the recently reported works (tabulated in Table S1), which may result from some following advantages. (Ⅰ) The totally separated excitation source (light) and the signal readout (electricity) endows PEC detection with an almost zero background.[17-22] (Ⅱ) The co-sensitization strategy is already simple and sensitive enough to detect the trace targets.[36,37] Furthermore, a high co-sensitization efficiency was achieved in our design by coupling CdSe QDs with the ternary TiO_2/g-C_3N_4/CdS nanocomposite with a cascade energy level arrangement, resulting in a superior PEC reaction with sufficient light absorption, effective charge separation, and rapid electron transfer. (Ⅲ) Other advantages, such as the large specific surface area of the ternary nanocomposite, the specific recognition of the complementary DNA chains[46], as well as the optimized experimental conditions, also favor our biosensor with a better analytical performance for the evaluation of T4 PNK.

Kinase Inhibition Assay

It is well established that ADP and $(NH_4)_2SO_4$ are common inhibitors[11,14,16] to evaluate the T4 PNK inhibition activity. ADP inhibits the T4 PNK activity by transferring phosphate group from DNA to ADP molecules, and $(NH_4)_2SO_4$ can change the nature of DNA and T4 PNK to inhibit T4 PNK activity. The concentration of T4 PNK (1.0 U mL^{-1}) remained unchanged in the inhibition test with different concentrations of inhibitors. The intensity displayed a gradual decrease with the increasing amounts of ADP or $(NH_4)_2SO_4$ (Shown in Figure 6) with the half-maximal inhibition concentration (IC_{50}) estimated to be 1.25 and 5.0 mM, respectively. These results are similar to 1.0 and 7.5 mM previously reported by Lin et al.[39] and Gao et al.[47], and evidently indicated the feasibility of this constructed PEC platform to screen the inhibitors and evaluate the corresponding inhibition effect.

Specificity, Repeatability, and Storage Stability

Some interfering enzymes containing adenylate kinase (AK), EcoRV, BamHI, EcoRI, and heat-inactivated T4 PNK were chosen to conduct assays under identical conditions to assess the selectivity of this prepared platform.[11,48] As shown in Figure 7, apart from the photocurrent of T4 PNK alone and the mixed enzymes containing T4 PNK displaying significantly enhanced intensities (60.00% and 61.25%), all others showed relatively low intensities (1.25%-3.75%). The results signified that the proposed platform possessed a selectivity for T4 PNK catalyzing phosphorylation reaction.

Five FTO electrodes produced in the same batch were utilized to evaluate the repeatability of the assay. The detection relative standard deviation (RSD) between same batch and different batches at 0.0001, 0.001 and 0.01 U mL^{-1} of target were

corresponding estimated as low as 2.03%, 3.43%, 2.98% and 3.81%, 4.63%, 4.17%. These results demonstrated that this PEC platform showed good repeatability.

The storage stability was studied by storing the constructed electrode at 4 °C for fifteen days, and the photocurrent only reduced 0.5% relative to the initial intensity, suggesting its excellent storage stability (Figure S4, Supporting Information).

CONCLUSIONS

In summary, a novel PEC platform was constructed based on co-sensitization effect between ternary TiO_2/g-C_3N_4/CdS nanocomposite and CdSe QDs with a cascade energy level arrangement to sensitively detect T4 PNK activity. As the matrix of this sensing platform, ternary TiO_2/g-C_3N_4/CdS nanocomposite was successfully synthetized and exhibited a cascade energy level arrangement with excellent photoelectric performances including sufficient light absorption, effective charge separation, and rapid electron transfer. As the sensitizers, CdSe QDs match the ternary nanocomposite with stepwise band-edge levels to achieve impactful co-sensitization efficiency. Under the optimal conditions, this proposed platform demonstrated the ultrasensitive determination of T4 PNK. In addition, the proposed PEC platform with high selectivity, good repeatability, and perfect stability can also serve as a potential tool for T4 PNK activity inhibitor screening, which may have a contribution for the discovery of anticancer drug.

ASSOCIATED CONTENT

Supporting Information

Materials, instruments, synthesis method of CdSe QDs and the corresponding characterizations, optimization experiments, storage stability experiment, and recently reported articles concerning T4 PNK detection. This material is available free of charge via the Internet at http://pubs.acs.org.

AUTHOR INFORMATION

Corresponding Authors

*E-mail: maochangjie@sina.com.

*E-mail: jjzhu@nju.edu.cn. Tel: + (86)2589687204.

Notes

The authors declare no competing financial interest.

ACKNOWLEDGMENTS

We thank the support from International Cooperation Foundation from Ministry of Science and Technology of China (2016YFE0130100). This work was also supported by the National Natural Science Foundation of China (Grant No. 21427807, 21575001).

REFERENCES

(1) Becker, A.; Hurwitz, J. The enzymatic cleavage of phosphate termini from polynucleotides. *J. Biol. Chem*. **1967**, 242, 936-950.

(2) Cameron, V.; Uhlenbeck, O. C. 3'-Phosphatase activity in T4 polynucleotide kinase. *Biochemistry* **1977**, 16, 5120-5126.

(3) Richardson, C. C. Phosphorylation of nucleic acid by an enzyme from T4 bacteriophage-infected Escherichia coli. *Proc. Natl. Acad. Sci. U.S.A.* **1965**, 54, 158-165.

(4) Sharma, S.; Doherty, K. M.; Brosh, R. M. Mechanisms of RecQ helicases in pathways of DNA metabolism and maintenance of genomic stability. *Biochem. J.* **2006**, 398, 319-337.

(5) Tahbaz, N.; Subedi, S.; Weinfeld, M. Role of polynucleotide kinase/phosphatase in mitochondrial DNA repair. *Nucleic Acids Res.* **2012**, 40, 3484-3495.

(6) Mereniuk, T. R.; Maranchuk, R. A.; Schindler, A.; Penner-Chea, J.; Freschauf, G. K.; Hegazy, S.; Lai, R.; Foley, E.; Weinfeld, M. Genetic screening for synthetic lethal partners of polynucleotide kinase/phosphatase: potential for targeting SHP-1-depleted cancers. *Cancer Res.* **2012**, 72, 5934-5944.

(7) Whitehouse, C. J.; Taylor, R. M.; Thistlethwaite, A.; Zhang, H.; Busheri, F. M.; Lasko, D. D.; Weinfeld, M.; Caldecott, K. W. XRCC1 stimulates human polynucleotide kinase activity at damaged DNA termini and accelerates DNA single-strand break repair. *Cell* **2001**, 104, 107-117.

(8) Feng, C.; Wang, Z. H.; Chen, T. S.; Chen, X. X.; Mao, D. S.; Zhao, J.; Li, G. X. A

dual-enzyme-assisted three-dimensional DNA walking machine using T4 polynucleotide kinase as activators and application in polynucleotide kinase assays. *Anal. Chem.* **2018**, 90, 2810-2815.

(9) Bernstein, N. K.; Williams, R. S.; Rakovszky, M. L.; Cui, D. D.; Green, R.; Karimi-Busheri, F.; Mani, R. S.; Galicia, S.; Koch, C. A.; Cass, C. E.; Durocher, D.; Weinfeld, M.; Glover, J. N. M. The molecular architecture of the mammalian DNA repair enzyme, polynucleotide kinase. *Mol. Cell* **2005**, 17, 657-670.

(10) Phillips, D. H.; Arlt, V. M. The ^{32}P-postlabeling assay for DNA adducts. *Nat. Protoc.* **2007**, 2, 2772-2781.

(11) Wang, L. J.; Zhang, Q. Y.; Tang, B.; Zhang, C. Y. Single-molecule detection of polynucleotide kinase based on phosphorylation-directed recovery of fluorescence quenched by Au nanoparticles. *Anal. Chem.* **2017**, 89, 7255-7261.

(12) Wang, G. F.; He, X. P.; Xu, G.; Chen, L.; Zhu, Y. H.; Zhang, X. J.; Wang, L. Detection of T4 polynucleotide kinase activity with immobilization of TiO_2 nanotubes and amplification of Au nanoparticles. *Biosens. Bioelectron.* **2013**, 43, 125-130.

(13) Jiang, H. X.; Kong, D. M.; Shen, H. X. Amplified detection of DNA ligase and polynucleotide kinase/phosphatase on the basis of enrichment of catalytic G-quadruplex DNAzyme by rolling circle amplification. *Biosens. Bioelectron.* **2014**, 55, 133-138.

(14) Hou, T.; Wang, X. Z.; Liu, X. J.; Lu, T. T.; Liu, S. F.; Li, F. Amplified detection of T4 polynucleotide kinase activity by the coupled λ exonuclease cleavage reaction

and catalytic assembly of bimolecular beacons. *Anal. Chem.* **2014**, 86, 884-890.

(15) He, H. Z.; Leung, K. H.; Wang, W.; Chan, D. S. H.; Leung, C. H.; Ma, D. L. Label-free luminescence switch-on detection of T4 polynucleotide kinase activity using a G-quadruplex-selective probe. *Chem. Commun.* **2014**, 50, 5313-5315.

(16) Lin, L.; Liu, Y.; Zhao, X.; Li, J. H. Sensitive and rapid screening of T4 polynucleotide kinase activity and inhibition based on coupled exonuclease reaction and graphene oxide platform. *Anal. Chem.* **2011**, 83, 8396-8402.

(17) Tu, W. W.; Wang, Z. Y.; Dai, Z. H. Selective photoelectrochemical architectures for biosensing: design, mechanism and responsibility. *Trends Anal. Chem.* **2018**, 105, 470-483.

(18) Zhang, G. Y.; Shan, D.; Dong, H. F.; Cosnier, S.; Al-Ghanim, K. A.; Ahmad, Z.; Mahboob, S.; Zhang, X. J. DNA-mediated nanoscale metal-organic frameworks for ultrasensitive photoelectrochemical enzyme-free immunoassay. *Anal. Chem.* **2018**, 90, 12284-12291.

(19) Zang, Y.; Fan, J.; Ju, Y.; Xue, H. G.; Pang, H. Current advances in semiconductor nanomaterial-based photoelectrochemical biosensing. *Chem. Eur. J.* **2018**, 24, 14010-14027.

(20) Li, M. J.; Xiong, C.; Zheng, Y. N.; Liang, W. B.; Yuan, R.; Chai, Y. Q. Ultrasensitive photoelectrochemical biosensor based on DNA tetrahedron as nanocarrier for efficient immobilization of CdTe QDs-methylene blue as signal probe with near-zero background noise. *Anal. Chem.* **2018**, 90, 8211-8216.

(21) Liu, S. S.; He, P.; Hussain, S.; Lu, H.; Zhou, X.; Lv, F. T.; Liu, L. B.; Dai, Z. H.;

Wang, S. Conjugated polymer-based photoelectrochemical cytosensor with turn-on enable signal for sensitive cell detection. *ACS Appl. Mater. Interfaces* **2018**, 10, 6618-6623.

(22) Zhao, W. W.; Xu, J. J.; Chen, H. Y. Photoelectrochemical bioanalysis: the state of the art. *Chem. Soc. Rev.* **2015**, 44, 729-741.

(23) Li, L.; Zheng, X. X.; Huang, Y. Z.; Zhang, L. N.; Cui, K.; Zhang, Y.; Yu, J. H. Addressable TiO_2 nanotubes functionalized paper-based cyto-sensor with photocontrollable switch for highly-efficient evaluating surface protein expressions of cancer cells. *Anal. Chem.* **2018**, DOI: 10.1021/acs.analchem.8b02849.

(24) Huo, H. H.; Xu, Z. D.; Zhang, T.; Xu, C. L. Ni/CdS/TiO_2 nanotube array heterostructures for high performance photoelectrochemical biosensing. *J. Mater. Chem. A*, **2015**, 3, 5882-5888.

(25) Çakıroğlu, B.; Özacar, M. A self-powered photoelectrochemical glucose biosensor based on supercapacitor Co_3O_4-CNT hybrid on TiO_2. *Biosens. Bioelectron.* **2018**, 119, 34-41.

(26) Li, X.; Zhu, L. S.; Zhou, Y. L.; Yin, H. S.; Ai, S. Y. Enhanced photoelectrochemical method for sensitive detection of protein kinase a activity using TiO_2/g-C_3N_4, PAMAM dendrimer, and alkaline phosphatase. *Anal. Chem.* **2017**, 89, 2369-2376.

(27) Sun, B.; Dong, J.; Cui, L.; Feng, T. T.; Zhu, J. J.; Liu, X. H.; Ai, S. Y. A dual signal-on photoelectrochemical immunosensor for sensitively detecting target avian viruses based on AuNPs/g-C_3N_4 coupling with CdTe quantum dots and in situ

enzymatic generation of electron donor. *Biosens. Bioelectron.* **2019**, 124-125, 1-7.

(28) Wang, H. Y.; Zhang, Q. H.; Yin, H. S.; Wang, M. H.; Jiang, W. J.; Ai, S. Y. Photoelectrochemical immunosensor for methylated RNA detection based on g-C_3N_4/CdS quantum dots heterojunction and phos-tag-biotin. *Biosens. Bioelectron.* **2017**, 95, 124-130.

(29) Zazpe, R.; Sopha, H, Prikryl, J.; Krbal, M.; Mistrik, J.; Dvorak, F.; Hromadko, L.; Macak, J. M. A 1D conical nanotubular TiO_2/CdS hetero-structure with superior photon-to-electron conversion. *Nanoscale* **2018**, 10, 16601-16612.

(30) Liang, J.; Wang, C. X.; Zhao, P. Y.; Wang, Y. R.; Ma, L. B.; Zhu, G. Y.; Hu, Y.; Lu, Z. P.; Xu, Z. R.; Ma, Y.; Chen, T.; Tie, Z. X.; Liu, J.; Jin, Z. Interface engineering of anchored ultrathin TiO_2/MoS_2 heterolayers for highly-efficient electrochemical hydrogen production. *ACS Appl. Mater. Interfaces* **2018**, 10, 6084-6089.

(31) Fan, D. W.; Ren, X.; Wang, H. Y.; Wu, D.; Zhao, D.; Chen, Y. C.; Wei, Q.; Du, B. Ultrasensitive sandwich-type photoelectrochemical immunosensor based on CdSe sensitized La-TiO_2 matrix and signal amplification of polystyrene@Ab_2 composites. *Biosens. Bioelectron.* **2017**, 87, 593-599.

(32) Cai, J.; Sheng, P. T.; Zhou, L. P.; Shi, L.; Wang, N. Y.; Cai, Q. Y. Label-free photoelectrochemical immunosensor based on CdTe/CdS co-sensitized TiO_2 nanotube array structure for octachlorostyrene detection. *Biosens. Bioelectron.* **2013**, 50, 66-71.

(33) Shen, S. H.; Chen, J.; Wang, M.; Sheng, X.; Chen, X. Y.; Feng, X. J.; Mao, S.

Titanium dioxide nanostructures for photoelectrochemical applications. *Prog. Mater. Sci.* **2018**, 98, 299-385.

(34) Wang, B.; Cao, J. T.; Dong, Y. X.; Liu, F. R.; Fu, X. L.; Ren, S. W.; Ma, S. H.; Liu, Y. M. An in situ electron donor consumption strategy for photoelectrochemical biosensing of proteins based on ternary $Bi_2S_3/Ag_2S/TiO_2$ NT arrays. *Chem. Commun.* **2018**, 54, 806-809.

(35) Liu, X. Q.; Liu, P. P.; Tang, Y. F.; Yang, L. W.; Li, L. L.; Qi, Z. C.; Li, D. L.; Wong, D. K. Y. A photoelectrochemical aptasensor based on a 3D flower-like TiO_2-MoS_2-gold nanoparticle heterostructure for detection of kanamycin. *Biosens. Bioelectron*. **2018**, 112, 193-201.

(36) Fan, G. C.; Han, L.; Zhu, H.; Zhang, J. R.; Zhu, J. J. Ultrasensitive photoelectrochemical immunoassay for matrix metalloproteinase-2 detection based on CdS:Mn/CdTe cosensitized TiO_2 nanotubes and signal amplification of SiO_2@Ab_2 conjugates. *Anal. Chem.* **2014**, 86, 12398-12405.

(37) Fan, G. C.; Ren, X. L.; Zhu, C.; Zhang, J. R.; Zhu, J. J. A new signal amplification strategy of photoelectrochemical immunoassay for highly sensitive interleukin-6 detection based on TiO_2/CdS/CdSe dual co-sensitized structure. *Biosens. Bioelectron.* **2014**, 59, 45-53.

(38) Wang, W.; Fang, J. J.; Shao, S. F.; Lai, M.; Lu, C. H. Compact and uniform TiO_2@g-C_3N_4 core-shell quantum heterojunction for photocatalytic degradation of tetracycline antibiotics. *Appl. Catal. B-Environ*. **2017**, 217, 57-64.

(39) Lin, L.; Liu, Y.; Yan, J.; Wang, X. S.; Li, J. H. Sensitive nanochannel biosensor

for T4 polynucleotide kinase activity and inhibition detection. *Anal. Chem.* **2013**, 85, 334-340.

(40) Maity, P.; Debnath, T.; Chopra, U.; Ghosh, H. N. Cascading electron and hole transfer dynamics in a CdS/CdTe core-shell sensitized with bromo-pyrogallol red (Br-PGR): slow charge recombination in type II regime. *Nanoscale* **2015**, 7, 2698-2707.

(41) Tang, Q.; Meng, X. F.; Wang, Z. Y.; Zhou, J. W.; Tang, H. One-step electrospinning synthesis of TiO_2/g-C_3N_4 nanofibers with enhanced photocatalytic properties. *Appl. Surf. Sci.* **2018**, 430, 252-262.

(42) Zhong, R. Y.; Zhang, Z. S.; Yi, H. Q.; Zeng, L.; Tang, C.; Huang, L. M.; Gu, M. Covalently bonded 2D/2D O-g-C_3N_4/TiO_2 heterojunction for enhanced visible-light photocatalytic hydrogen evolution. *Appl. Catal. B-Environ.* **2018**, 237, 1130-1138.

(43) Chu, J. Y.; Han, X. J.; Yu, Z.; Du, Y. C.; Song, B.; Xu, P. Highly efficient visible-light-driven photocatalytic hydrogen production on CdS/Cu_7S_4/g-C_3N_4 ternary heterostructures. *ACS Appl. Mater. Interfaces* **2018**, 10, 20404-20411.

(44) Lee, L. L.; Lo, Y. S. Highly efficient quantum-dot-sensitized solar cell based on co-sensitization of CdS/CdSe. *Adv. Funct. Mater*. **2009**, 19, 604-609.

(45) Yang, Z. J.; Cao, Y.; Li, J.; Lu, M. M.; Jiang, Z. K.; Hu, X. Y. Smart CuS nanoparticles as peroxidase mimetics for the design of novel label-free chemiluminescent immunoassay. *ACS Appl. Mater. Interfaces* **2016**, 8, 12031-12038.

(46) Zhao, W. W.; Xu, J. J.; Chen, H. Y. Photoelectrochemical DNA biosensors. *Chem.*

Rev. **2014**, 114, 7421-7411.

(47) Gao, M. X.; Guo, J. J.; Song, Y. L.; Zhu, Z.; Yang, C. Y. J. Detection of T4 polynucleotide kinase via allosteric aptamer probe platform. *ACS Appl. Mater. Interfaces* **2017**, 9, 38356-38363.

(48) Zhang, H.; Zhao, Z.; Lei, Z.; Wang, Z. X. Sensitive detection of polynucleotide kinase activity by paper-based fluorescence assay with λ exonuclease assistance. *Anal. Chem.* **2016**, 88, 11358-11363.

FIGURE CAPTIONS

Scheme 1. (A) Schematic exhibition of fabrication process of the sensing platform and protocol of the co-sensitization amplification PEC assay; (B) Photogenerated electron-hole transfer mechanism of the co-sensitization strategy with a cascade energy level arrangement.

Figure 1. SEM image (A), TEM image (B1), HRTEM images (B2 and B3), XRD spectra (C), and STEM (D) of the as-synthesized ternary TiO_2/g-C_3N_4/CdS nanocomposite.

Figure 2. Feasibility of the co-sensitization amplification strategy. Three systems were cosensitized with constant amounts of CdSe QDs. Inserted diagram at right side shows the corresponding real photocurrent responses.

Figure 3. XPS analysis of (a) Ti 2p and (b) O 1s of TiO_2, TiO_2/C_3N_4, and TiO_2/g-C_3N_4/CdS; (c) C 1s and (d) N 1s of C_3N_4, TiO_2/C_3N_4, and TiO_2/g-C_3N_4/CdS; (e) Cd 3d and (f) S 2p of CdS, and TiO_2/g-C_3N_4/CdS.

Figure 4. (A). Photocurrent responses of FTO (a), FTO/TiO_2 (b), FTO/TiO_2/g-C_3N_4 (c), FTO/TiO_2/g-C_3N_4/CdS (d), FTO/TiO_2/g-C_3N_4/CdS/capture-DNA_3/MCH (e), FTO/TiO_2/g-C_3N_4/CdS/capture-DNA_3/MCH/DNA_2-CdSe (f), FTO/TiO_2/g-C_3N_4/CdS/capture-DNA_3/MCH/CdSe (g); (B) Nyquist plots of EIS measurements for bare FTO (a), FTO/TiO_2/g-C_3N_4/CdS (b), FTO/TiO_2/g-C_3N_4/CdS/capture-DNA_3/MCH (c), FTO/TiO_2/g-C_3N_4/CdS/capture-DNA_3/MCH/DNA_2-CdSe (d), FTO/TiO_2/g-C_3N_4/CdS/capture-DNA_3/MCH/CdSe (e).

Figure 5. (A). Photocurrent responses of the PEC platform to different concentrations

of T4 PNK from 0.0001 U mL^{-1} to 1 U mL^{-1}. (B). Corresponding photocurrents versus various T4 PNK concentrations for the sensing system. The inset shows the linearity of the photocurrent response against the logarithm of target dose (n=5 for each date point).

Figure 6. Inhibitory effects of (A) ADP, (B) $(NH_4)_2SO_4$ on T4 PNK activity with a T4 PNK concentration of 1.0 U mL^{-1}.

Figure 7. Selectivity of the PEC platform for T4 PNK activity detection. The concentration of inactive T4 PNK was 0.1 U mL^{-1} and others were 0.01 U mL^{-1}.

For TOC only

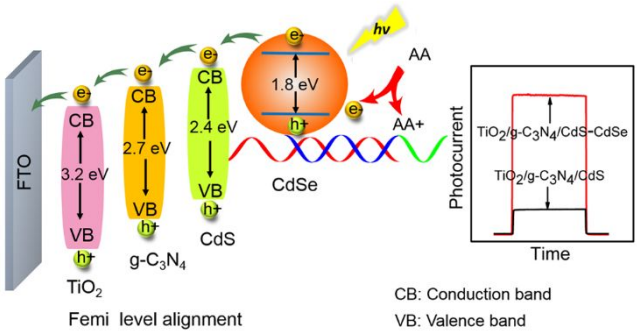
FTO
CB
3.2 eV
VB
TiO2
CB
2.7 eV
VB
g-C3N4
CB
2.4 eV
VB
CdS
1.8 eV
CdSe
hν
AA
AA+
Photocurrent
TiO2/g-C3N4/CdS-CdSe
TiO2/g-C3N4/CdS
Time
Femi level alignment
CB: Conduction band
VB: Valence band

Scheme 1

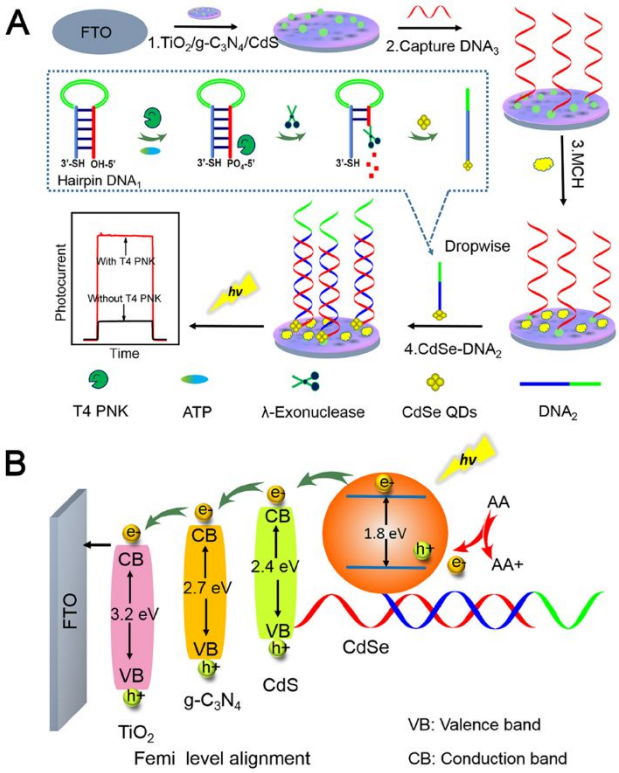
A
FTO
1.TiO2/g-C3N4/CdS
2.Capture DNA3
3'-SH OH-5'
3'-SH PO4-5'
3'-SH
Hairpin DNA1
3.MCH
Dropwise
Photocurrent
With T4 PNK
Without T4 PNK
Time
hv
4.CdSe-DNA2
T4 PNK
ATP
λ-Exonuclease
CdSe QDs
DNA2
B
hv
AA
AA+
1.8 eV
2.4 eV
2.7 eV
3.2 eV
CB
VB
FTO
TiO2
g-C3N4
CdS
CdSe
Femi level alignment
VB: Valence band
CB: Conduction band

Figure 1

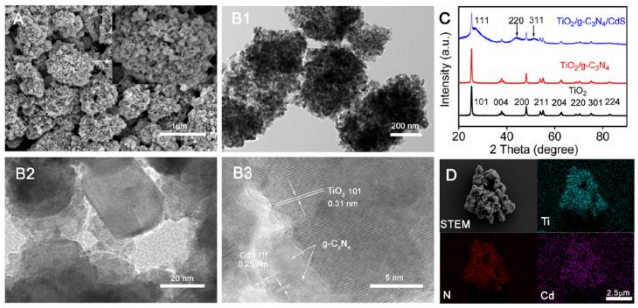
A
B1
200 nm
C
111
220
311
TiO_2/g-C_3N_4/CdS
TiO_2/g-C_3N_4
TiO_2
101 004 200 211 204 220 301 224
Intensity (a.u.)
20
40
60
80
2 Theta (degree)
B2
20 nm
B3
TiO_2 101
0.31 nm
g-C_3N_4
CdS 111
0.25 nm
5 nm
D
STEM
Ti
N
Cd
2.5μm

Figure 2

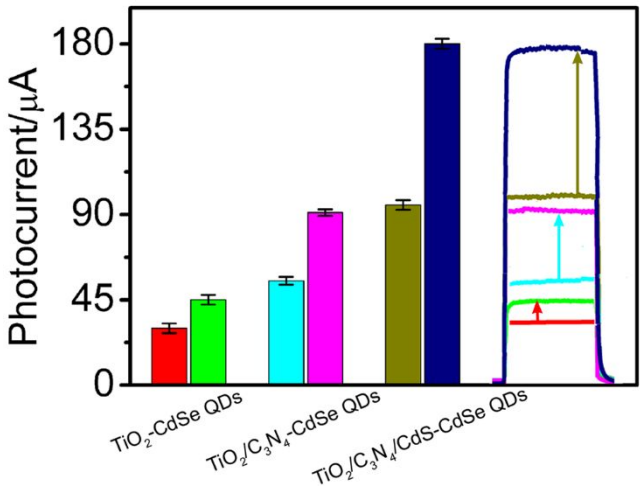
Photocurrent/μA
180
135
90
45
0
TiO2-CdSe QDs
TiO2/C3N4-CdSe QDs
TiO2/C3N4/CdS-CdSe QDs

Figure 3

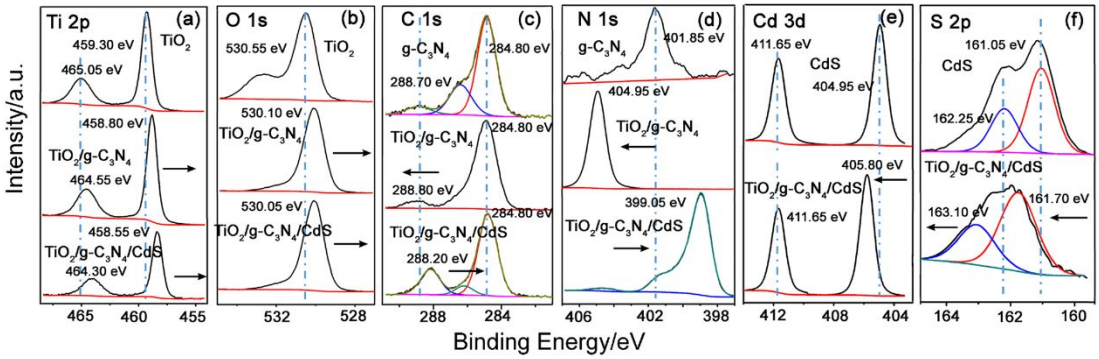
Ti 2p
(a)
459.30 eV
TiO2
465.05 eV
458.80 eV
TiO2/g-C3N4
464.55 eV
458.55 eV
TiO2/g-C3N4/CdS
464.30 eV
465
460
455
O 1s
(b)
530.55 eV
TiO2
530.10 eV
TiO2/g-C3N4
530.05 eV
TiO2/g-C3N4/CdS
532
528
C 1s
(c)
g-C3N4
284.80 eV
288.70 eV
TiO2/g-C3N4
284.80 eV
288.80 eV
284.80 eV
TiO2/g-C3N4/CdS
288.20 eV
288
284
N 1s
(d)
g-C3N4
401.85 eV
404.95 eV
TiO2/g-C3N4
399.05 eV
TiO2/g-C3N4/CdS
406
402
398
Cd 3d
(e)
411.65 eV
CdS
404.95 eV
405.80 eV
TiO2/g-C3N4/CdS
411.65 eV
412
408
404
S 2p
(f)
161.05 eV
CdS
162.25 eV
TiO2/g-C3N4/CdS
161.70 eV
163.10 eV
164
162
160
Intensity/a.u.
Binding Energy/eV

Figure 4

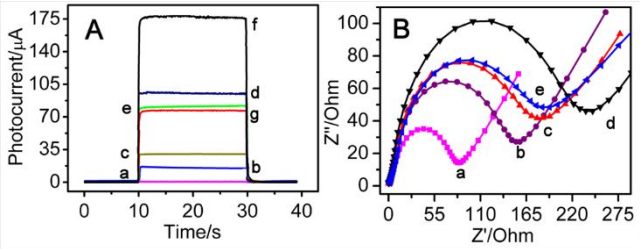
A
Photocurrent/μA
175
140
105
70
35
0
0
10
20
30
40
Time/s
a
b
c
d
e
f
g
B
Z''/Ohm
100
80
60
40
20
0
0
55
110
165
220
275
Z'/Ohm
a
b
c
d
e

Figure 5

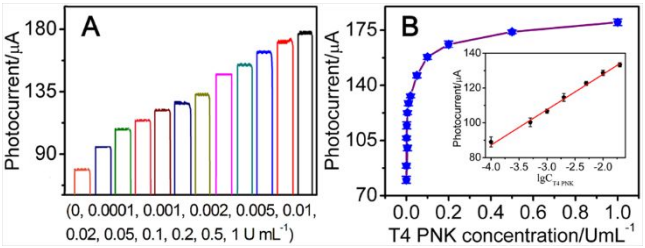
A
Photocurrent/μA
180
135
90
(0, 0.0001, 0.001, 0.002, 0.005, 0.01, 0.02, 0.05, 0.1, 0.2, 0.5, 1 U mL-1)
B
Photocurrent/μA
175
140
105
70
0.0 0.2 0.4 0.6 0.8 1.0
T4 PNK concentration/UmL-1
140
120
100
80
-4.0 -3.5 -3.0 -2.5 -2.0

Figure 6

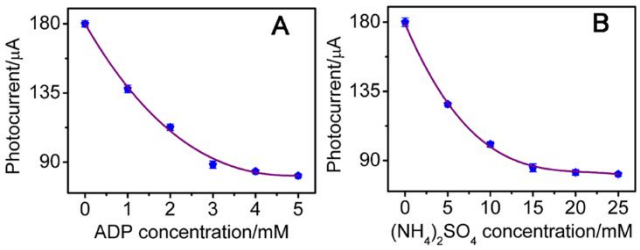
A
B
Photocurrent/μA
180
135
90
0 1 2 3 4 5
ADP concentration/mM
0 5 10 15 20 25
(NH4)2SO4 concentration/mM

Figure 7

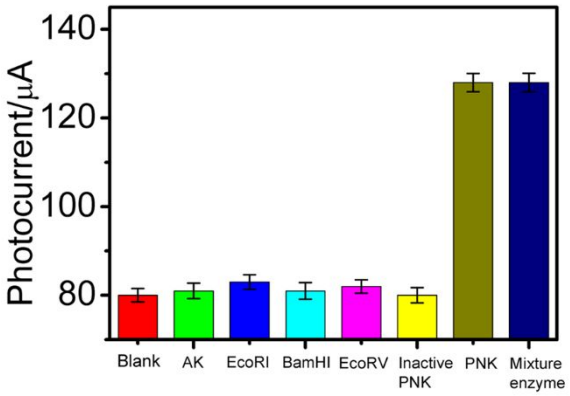
Photocurrent/μA
140
120
100
80
Blank
AK
EcoRI
BamHI
EcoRV
Inactive PNK
PNK
Mixture enzyme

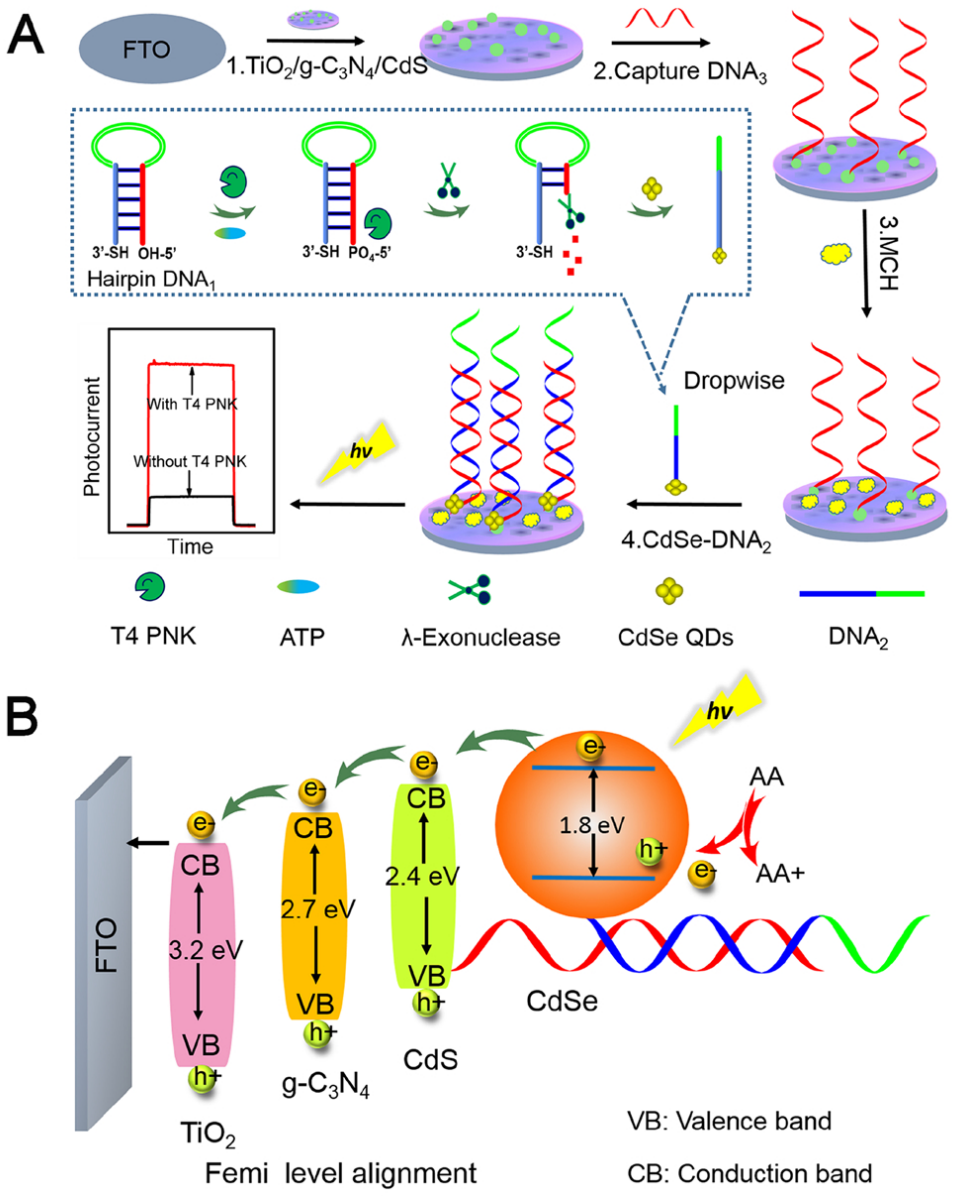

Scheme 1. Schematic exhibition of fabrication process of the sensing platform and protocol of the co-sensitization amplification PEC assay.

84x102mm (300 x 300 DPI)

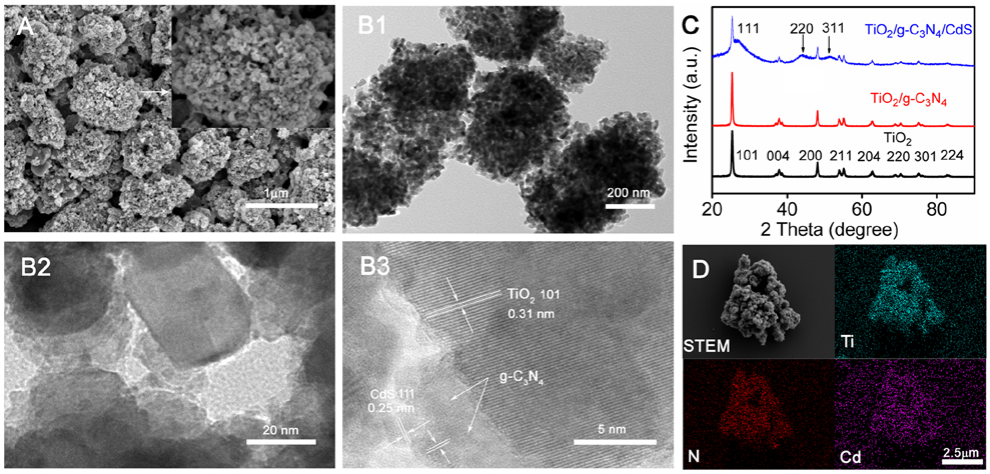

Figure 1. SEM image (A), TEM image (B1), HRTEM images (B2 and B3), XRD spectra (C), and STEM (D) of the as-synthesized ternary TiO2/g-C3N4/CdS nanocomposite.

84x40mm (300 x 300 DPI)

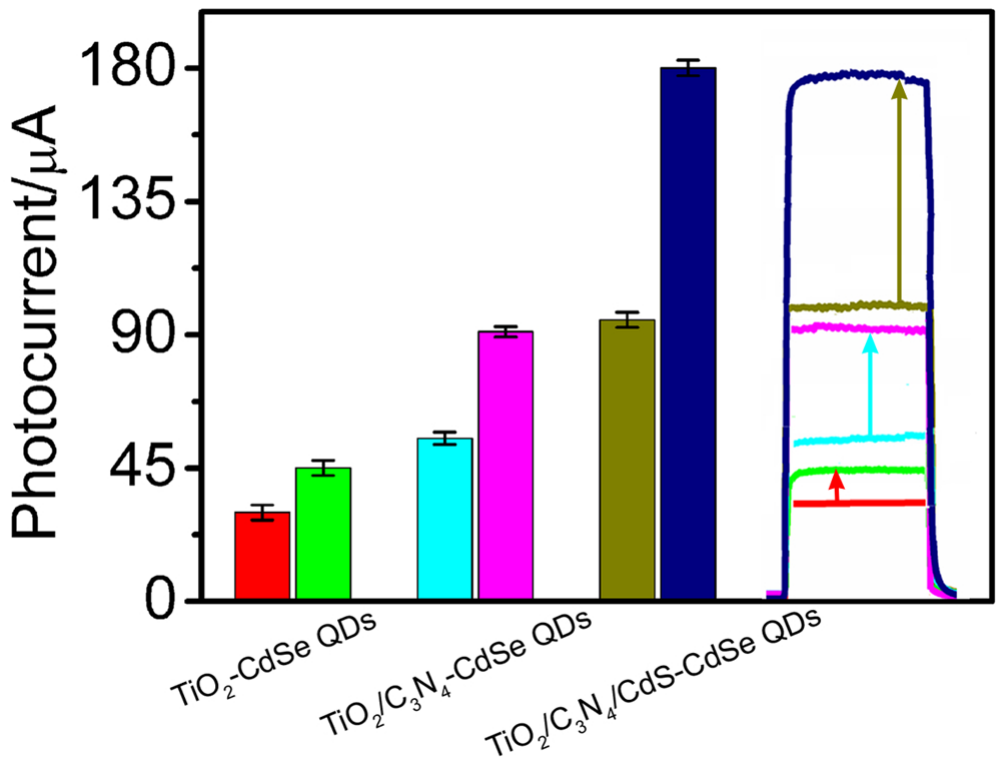

Figure 2. Feasibility of the co-sensitization amplification strategy. Three systems were cosensitized with constant amounts of CdSe QDs. Inserted diagram at right side shows the corresponding real photocurrent responses.

84x64mm (300 x 300 DPI)

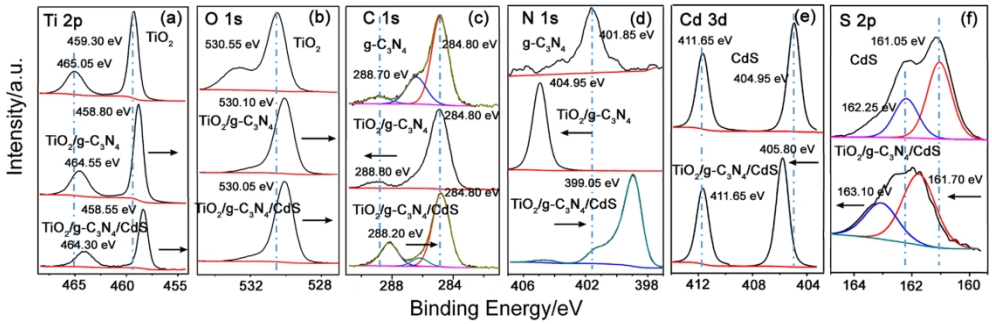

Figure 3. XPS analysis of (a) Ti 2p and (b) O 1s of TiO2, TiO2/C3N4, and TiO2/g-C3N4/CdS; (c) C 1s and (d) N 1s of C3N4, TiO2/C3N4, and TiO2/g-C3N4/CdS; (e) Cd 3d and (f) S 2p of CdS, and TiO2/g-C3N4/CdS.

177x57mm (300 x 300 DPI)

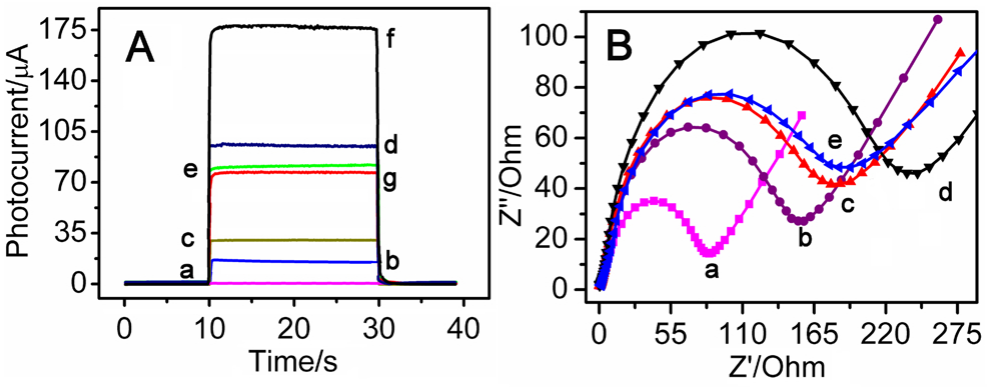

Figure 4. (A). Photocurrent responses of FTO (a), FTO/TiO2 (b), FTO/TiO2/g-C3N4 (c), FTO/TiO2/g-C3N4/CdS (d), FTO/TiO2/g-C3N4/CdS/capture-DNA3/MCH (e), FTO/TiO2/g-C3N4/CdS/capture-DNA3/MCH/DNA2-CdSe (f), FTO/TiO2/g-C3N4/CdS/capture-DNA3/MCH/CdSe (g); (B) Nyquist plots of EIS measurements for bare FTO (a), FTO/TiO2/g-C3N4/CdS (b), FTO/TiO2/g-C3N4/CdS/capture-DNA3/MCH (c), FTO/TiO2/g-C3N4/CdS/capture-DNA3/MCH/DNA2-CdSe (d), FTO/TiO2/g-C3N4/CdS/capture-DNA3/MCH/CdSe (e).

84x32mm (300 x 300 DPI)

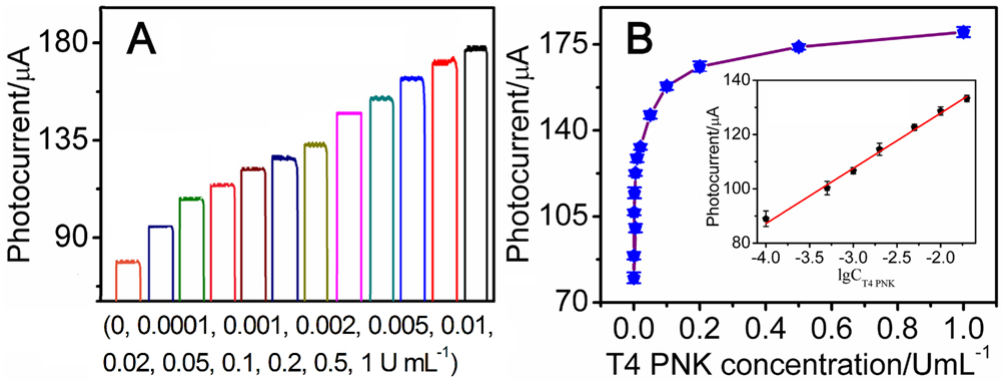

Figure 5. (A). Photocurrent responses of the PEC platform to different concentrations of T4 PNK from 0.0001 U mL-1 to 1 U mL-1. (B). Corresponding photocurrents versus various T4 PNK concentrations for the sensing system. The inset shows the linearity of the photocurrent response against the logarithm of target dose (n=5 for each date point).

84x32mm (300 x 300 DPI)

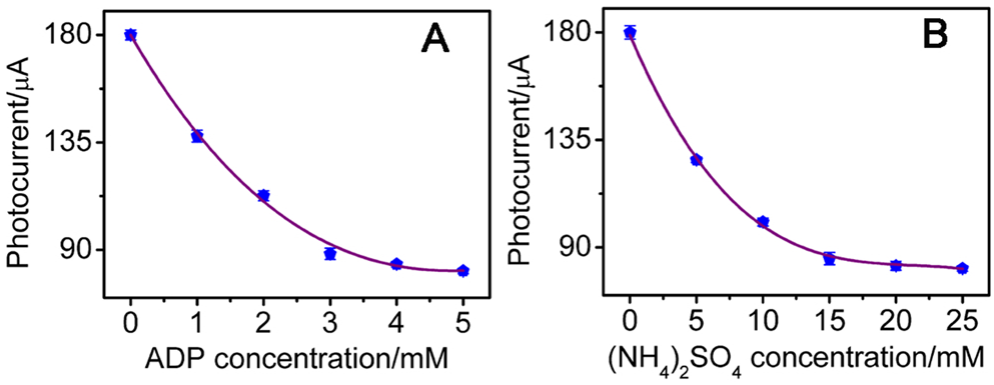

Figure 6. Inhibitory effects of (A) ADP, (B) (NH4)2SO4 on T4 PNK activity with a T4 PNK concentration of 1.0 U mL−1.

84x33mm (300 x 300 DPI)

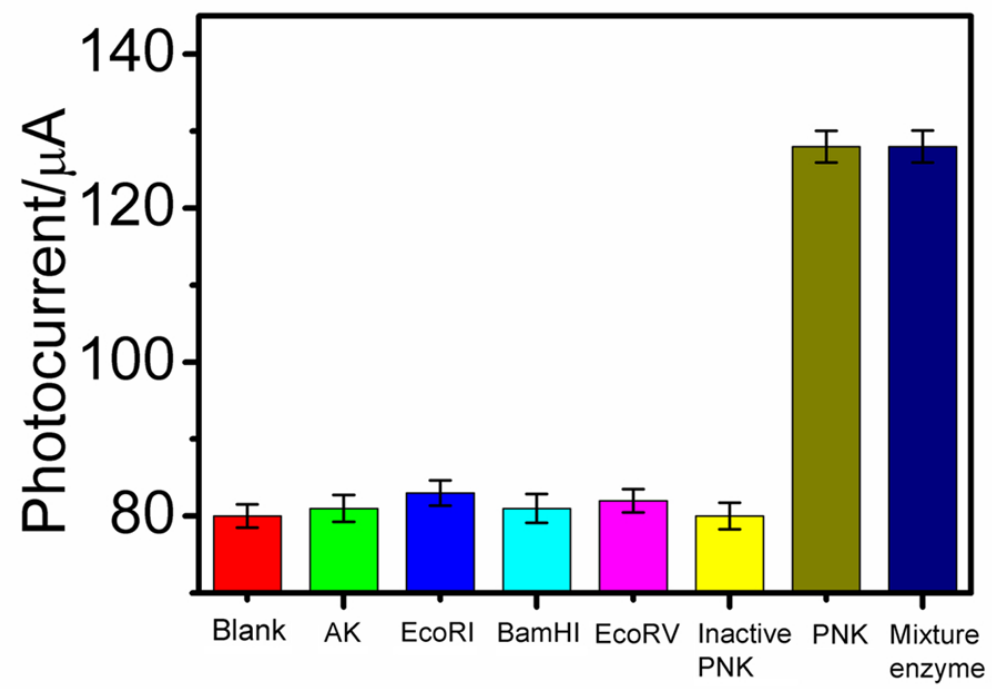

Figure 7. Selectivity of the PEC platform for T4 PNK activity detection. The concentration of inactive T4 PNK was 0.1 U mL-1 and others were 0.01 U mL-1.

76x52mm (300 x 300 DPI)

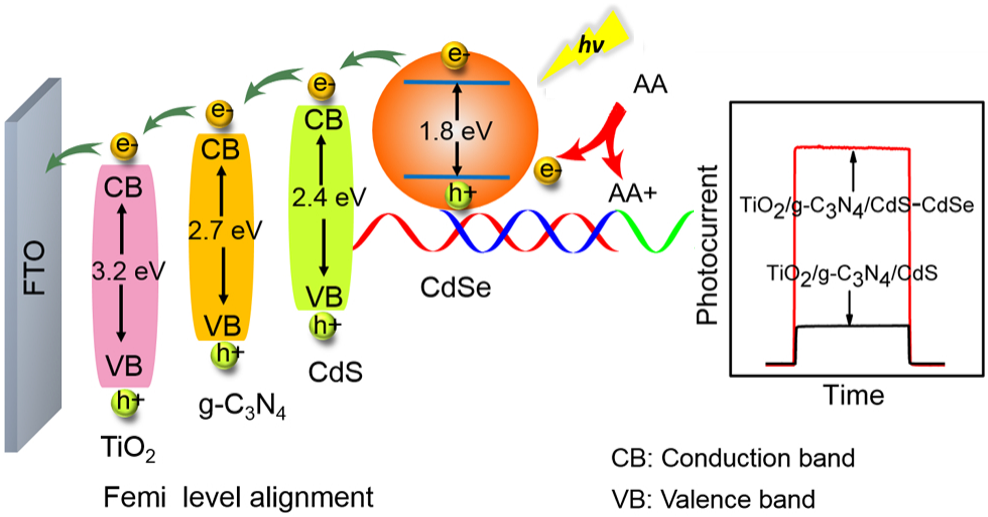

for TOC only

84x47mm (300 x 300 DPI)